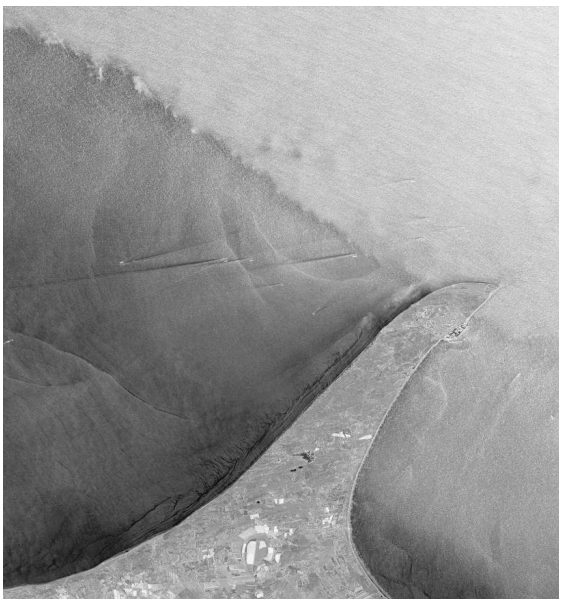

Sea Surface Current Measurements Using Along-Track Interferometric SAR

ANIS ELYOUNCHA

Department of Space, Earth and Environment
CHALMERS UNIVERSITY OF TECHNOLOGY
Göteborg, Sweden 2018

THESIS FOR THE DEGREE OF LICENTIATE OF ENGINEERING

Sea Surface Current Measurements Using Along-Track Interferometric SAR

ANIS ELYOUNCHA

Department of Space, Earth and Environment
Division of Microwave and Optical Remote Sensing
CHALMERS UNIVERSITY OF TECHNOLOGY

Göteborg, Sweden 2018

Sea Surface Current Measurements Using Along-Track Interferometric SAR
ANIS ELYOUNCHA

Department of Space, Earth and Environment
Division of Microwave and Optical Remote Sensing
Chalmers University of Technology
SE-412 96 Göteborg
Sweden
Telephone: +46 (0)31-772 2235

Cover:
The Kattegat-Skagerrak front at Skagen where the outflow of the brackish Baltic Sea water meets the saline North Sea water. The image illustrates how ocean surface features are imaged by the Synthetic Aperture Radar TerraSAR-X. Copyright DLR 2014.

Chalmers Reproservice
Göteborg, Sweden 2018

Sea Surface Current Measurements Using Along-Track Interferometric SAR
Thesis for the degree of Licentiate of Engineering
ANIS ELYOUNCHA
Department of Space, Earth and Environment
Division of Microwave and Optical Remote Sensing
Chalmers University of Technology

ABSTRACT

Ocean currents affect the weather, the climate and the marine ecosystem. Observing ocean currents is important for understanding the upper-ocean layer dynamics and its interaction with the other components of the climate system. In-situ measurements are sparse and their deployment and maintenance is costly. Satellite remote sensing with large spatial coverage offers a good complement to the in-situ observations.

In this work we have studied the spaceborne Along-Track Interferometric SAR (ATI-SAR) for measuring sea surface currents. The measurement principle is based on the fact that the phase difference between two SAR acquisitions is directly related to radial (line-of-sight) velocity of the illuminated surface. Previous studies based on similar systems were carried out in areas with well defined and strong tidal currents ($\sim 1-3\ m\ s^{-1}$). In this work we demonstrate the capability of ATI-SAR, through several study cases, in areas with weak currents ($\leq 0.5\ m\ s^{-1}$). This is challenging for the satellite measurements of surface currents because it requires very accurate processing and retrieval algorithms. In addition, it has been found that wave motion contribution, systematically dominates the measured ATI-SAR radial velocity in these weak current areas. Estimation of the wave motion contribution relies on high-resolution and accurate wind data. Thus, a wind speed retrieval algorithm from SAR is needed to support the ATI-SAR current retrieval. We have shown that with an appropriate processing of the ATI-SAR phase and with applying the necessary corrections to the measured velocity a good agreement with ocean circulation models is achieved ($rmse \approx 0.1\ m\ s^{-1}$). These corrections include phase calibration and wind compensation to correct for instrument and geophysical systematic errors, respectively. Finally, a novel method for removing the wind direction ambiguity, based on the ATI-SAR phase, is presented. In previous methods, the wind ambiguity removal was based on external information, e.g. an atmospheric model or on visual observation of wind shadows.

Keywords: Along-track InSAR, Sea surface currents, Ocean remote sensing, Synthetic aperture radar, SAR.

ACKNOWLEDGEMENTS

First, I would like to express my sincere gratitude to my main supervisor Dr. Leif Eriksson, for giving me the opportunity to undertake this work, for the guidance, support and encouragement he has provided throughout the past 2.5 years. I would also like to specially thank my co-supervisor and examiner Prof. Lars Ulander, for the guidance, the fruitful discussions, the valuable advice and relevant inputs to my work. I am also grateful to my co-supervisors Dr. Göran Broström and Dr. Roland Romeiser for their feedback, suggestions and comments on my papers. I would like to thank all my colleagues in the department of Space, Earth and Environment for all kind of help, support and encouragement. Last but not the least, I am so thankful to my family: my mother, my sister and my brother for their continued support.

APPENDED PUBLICATIONS

This thesis is based on the work in the following appended Publications:

A. A. Elyouncha, L. E. B. Eriksson, R. Romeiser, G. K. Carvajal and L. M. H. Ulander, "Wind-wave Effect on ATI-SAR Measurements of Ocean Surface Currents in the Baltic Sea," *Proceedings of IEEE International Geoscience and Remote Sensing Symposium (IGARSS), Beijing, China, 10-15 July 2016, pp. 3982-3985*.

B. A. Elyouncha, L. E. B. Eriksson, R. Romeiser and L. M. H. Ulander, "Phase Calibration of TanDEM-X ATI-SAR Data for Sea Surface Velocity Measurements," *Proceedings of IEEE International Geoscience and Remote Sensing Symposium (IGARSS), Fort Worth, TX, USA, 23-28 July 2017, pp. 922-925*.

C. A. Elyouncha, L. E. B. Eriksson, R. Romeiser and L. M. H. Ulander, "Wind Direction Ambiguity Removal using Along-Track INSAR: A case study,". accepted for 2018 *IEEE International Geoscience and Remote Sensing Symposium (IGARSS), Valencia, Spain, 22-27 July 2018*.

D. A. Elyouncha, L. E. B. Eriksson, R. Romeiser and L. M. H. Ulander, "Measurements of Sea Surface Currents in the Baltic Sea Region using Spaceborne Along-Track InSAR,". Manuscript submitted to *IEEE Transactions on Geoscience and Remote Sensing*.

RELATED PAPERS

The author has contributed to the following paper which is related to the work in this thesis, but is not appended in this thesis:

I. Anis Elyouncha (2017).“High resolution ocean modelling for the validation of satellite sea surface currents retrieval”. Theoretical introduction for Master thesis project, 12 pages, Chalmers University of Technology, 2017.

CONTENTS

1 Introduction

Why observing the ocean is so important ?

The ocean is the largest sink for anthropogenic carbon dioxide (CO_2) released in the atmosphere, it absorbs about 30% of the annually emitted CO_2 (IPCC 2013). This carbon uptake contributes in reducing the rising of the CO_2 concentration in the atmosphere. The ocean is also the largest heat sink due to its large mass, high heat capacity and very low albedo which allows it to absorb a large amount of energy. This ocean heat uptake acts as a buffer for the global warming.

Presently, the Earth radiative budget is unbalanced, i.e. more energy enters the top of the atmosphere than leaves it. The largest amount of this excess energy goes into the ocean and warms it. This warming is slowing down the capacity of the ocean to absorb carbon, which has implications for the global carbon cycle and the climate system (IPCC 2013). The change in the ocean absorbing power is an active area of research. Since the beginning of the industrial era, increasing atmospheric carbon dioxide has led to an increase in ocean heat storage, warming of the ocean and consequently to sea level rise via expansion. Moreover, oceanic uptake of CO_2 has resulted in acidification of the ocean. In parallel to warming and acidification, a decrease in oxygen concentrations has been noticed in coastal waters and in the open ocean (IPCC 2013).

Ocean circulation plays an important role in the distribution of heat and CO_2. The connection between climate change and ocean circulation change has been established (e.g. Winton et al. 2013). The role of ocean circulation in carbon and heat uptake is an active field of research. For instance, (DeVries, Holzer, and Primeau 2017; Fletcher 2017) attributes the increase in the ocean's uptake of CO_2 during the 2000s to the weakening of the circulation in the upper ocean. The air-sea heat fluxes (latent and sensible) have a strong regional dependence and high uncertainties. These uncertainties hinder the detection of the change in global mean of the net air–sea heat flux due to anthropogenic climate change. Air-sea fluxes are either measured by the eddy covariance method or calculated from a bulk formula and measured bulk parameters. In eddy covariance method, the vertical flux is calculated from the covariance of the vertical wind velocity and the physical quantity of interest (e.g. temperature for heat flux). These measurements are sparse and expensive. In the bulk formula calculation, waves and ocean surface currents information is required (Dawe and L. A. Thompson 2006; Y. Wu, Zhai, and Wang 2017). Thus, observations of ocean currents can provide useful information for climate modelling and predictions.

Finally, the ocean, particularly in the coastal regions, is a host to many different human activities such as fishing, ship navigation, etc. For instance, oil pollution, plastic debris (NOAA 2016), tidal and wave energy is becoming of increasing concern. Thus, observing ocean currents, allows monitoring the advection of these pollutants and the optimization of ocean energy exploitation. In terms of societal impact of the ocean, with a large portion of the world's population living close to the coastline, ocean observation is essential for coastal hazards management.

Radar Remote Sensing of the ocean - Why Radar ?

Radar remote sensing of the ocean includes many applications such as weather forecasting, oil spill monitoring, sea ice detection, etc. (Elachi 1978; Kerbaol and Collard 2005; Gens 2008). Different radar systems used in remote sensing differ in design and processing which depends on the main application of the sensor. The most popular spaceborne radar sensors are the scatterometer, altimeter and Synthetic Aperture Radar (SAR). For a good review of their principles and applications see (Robinson 2004) and (Ulaby and Long 2014).

SAR, like the Real Aperture Radar (RAR), is weather and sun light independent. In addition, the main advantage of SAR w.r.t. RAR is its high spatial resolution and the fact that this resolution is independent of the distance between the sensor and the target. This allows Earth observation from space with resolutions approaching optical sensors resolutions.

Radar backscatter is sensitive to the dielectric (permittivity and conductivity) and geometric (surface roughness) properties of the illuminated surface. Over the ocean surface, the variation of the dielectric properties is relatively small. Moreover, at microwave frequencies the radar backscatter is not very sensitive to temperature and salinity. Thus the radar in this case is mainly used to sense the kinematic properties of the sea surface (K. Hasselmann, Raney, et al. 1985). The main driver for the sea surface roughness is the wind stress. Finally, SAR has proven to be particularly good at ocean features imaging and regional circulation patterns such as current features (Kudryavtsev et al. 2005), fronts, eddies (Johannessen, Kudryavtsev, et al. 2005), internal waves, gravity waves, upwelling zones, shallow water bathymetry (Alpers and Hennings 1984), etc.

Extracting ocean parameters from SAR data

It is relatively established now that SAR can be used for sensing several ocean phenomena and for extracting several oceanic parameters, from its data, such as wind speed (Horstmann et al. 2003), significant wave height (SchulzStellenfleth, König, and Lehner 2007), etc.

The oceanic parameters which have attracted most attention from researchers during last decades are the wave spectra (K. Hasselmann and S. Hasselmann 1991), (Engen et al. 1994) and the sea surface wind speed. From the wave spectra, several wave parameters can be extracted such as significant wave height, peak period (SchulzStellenfleth, König, and Lehner 2007). The sea surface wind speed retrieval has benefited from the similarity to scatterometry which is well established (Stoffelen and Anderson 1993; Bentamy et al. 2017). An overview of wind retrieval from SAR can be found in (Horstmann et al. 2003; Dagestad et al. 2012). There are still a few challenges to tackle in both fields, e.g. wind and wave direction ambiguity and high wind speed.

Although the first demonstrations of the feasibility of sea surface currents measurement using SAR have been published in the late eighties by (Goldstein and Zebker 1987) and (Goldstein, Zebker, and Barnett 1989), surface currents retrievals is still an on-going and challenging research field. This is because surface currents, as is shown in the appended papers, is highly dependent on accurate knowledge of other oceanic parameters namely wind fields and wave spectra in addition to instrument geometry and platform trajectory. Note that sea surface current speeds are one order of magnitude smaller than wind speed which puts stringent constraints on the precision and accuracy of the measurement. Moreover, currents are modulated by many other oceanic phenomena, e.g. internal waves, bathymetry, etc. which are difficult to model. There is, to my

knowledge, no universal retrieval algorithm for surface currents but rather ad-hoc solutions for limited study cases where the oceanographer expertise and judgement is still very much involved.

Surface scattering and RCS

A coherent radar, like SAR, measures essentially three parameters: backscattered power, time delay (range), and Doppler shift (by tracking the phase in time). The concept of the Radar Cross Section (RCS, σ) and the Normalized Radar Cross Section (NRCS, σ^o) is described in detail in many text books, e.g. (Richards, Scheer, and Holm 2010; Ulaby and Long 2014). σ^o is also called backscattering coefficient or just backscatter.

A given surface is defined by three parameters: the dielectric constant (permittivity and conductivity); roughness (height standard deviation); and slope (local incidence angle). Calculation of the σ^0 from a given surface requires a scattering model. A number of models have been developed in the last decades for the backscattering of electromagnetic waves from the ocean surface (Elachi and Brown 1977). The main models are: facet model (specular point model) valid at low incidence angles $0 - 20^o$ or very large slopes, Bragg model valid in intermediate incidence angle $20 - 60^o$ (Wright 1966) and the two-scale model (Valenzuela 1978) that combines the scattering from small scale (Bragg waves) and large scale ocean waves. A discussion of scattering models is beyond the scope of this text, the reader may refer to (Valenzuela 1968; Valenzuela 1978; Ulaby, Moore, and Fung 1986; Ulaby and Long 2014) for more details.

There are different surface scattering mechanisms, namely specular, diffuse and resonant. For a given dielectric constant, if the roughness is small relative to the wavelength (smooth surface), the dominant scattering mechanism is specular, i.e. the energy is scattered in one single direction and Snell's law applies. If the roughness is large relative to the wavelength (rough surface), the dominant scattering mechanism is diffuse, i.e. the energy is scattered in all directions with no dominant direction. If the surface is periodic, it gives a resonant scattering, i.e. the scattering is enhanced in given directions where the electromagnetic wave and the surface are in resonance. In a real ocean surface the scattering is a combination of all these mechanisms. However, one mechanism may dominate the others depending on the frequency, polarization and incidence angle.

Bragg scattering

Bragg scattering is a fundamental mechanism in SAR imaging of the sea surface. Thus, a brief description is provided in this section. The name Bragg comes from the analogy between scattering from ocean waves and the Bragg effect in X-ray diffraction. It is well known that the main contribution to the backscattered radar signal, at moderate incidence angles ($20 - 60^o$), is due to the Bragg scattering mechanism (see for example (Crombie 1955; Wright 1966; Plant 1990)). That is to say, if the sea surface is decomposed into its Fourier components, the backscattering is dominated by the surface Fourier component satisfying the Bragg condition (Robinson 2004)

$$\lambda_w = \frac{n\,\lambda_r}{2\,\sin\theta} \tag{1.1}$$

where λ_w, λ_r and θ are the ocean waves wavelength, the radar electromagnetic wavelength and the incidence angle respectively. Although, in principle, the resonance condition is satisfied

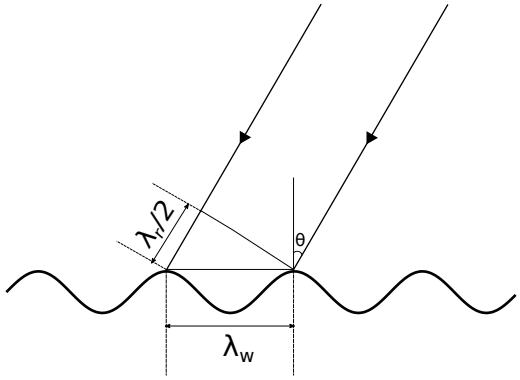

Figure 1.1. *Bragg scattering mechanism*

for all multiples of the wavelength, the first order ($n = 1$) is usually much larger than the higher orders. Thus in many texts the n is dropped from equation 1.1. In case of microwave radars, Bragg scattering originates from the gravity-capillary waves (also called ripples). For instance, for X-band with $\lambda_r = 0.031\ m$ and $\theta \approx 35^o$, $\lambda_w \approx 0.027\ m$.

Therefore, SAR measures mainly the backscatter of the Bragg waves, i.e. the NRCS is proportional to the wave spectral density at the Bragg wave number (Plant 1990). In absence of this component, the scattering is quasi-specular. Note that the slopes of the longer waves are usually too small, rarely exceeding 30^o (Cox and Munk 1954), to induce specular scattering toward the radar. This is, for instance, confirmed by observation of images of the sea surface covered by oil films that dampens the ripples and dramatically reduce the backscattered power. Note, however, that these Bragg waves are advected, modulated, strained, stretched, etc. by longer waves, currents, topography, etc. This is how these large features are detectable by SAR (Alpers, Ross, and Rufenach 1981). Finally, the Doppler shift measured by the SAR is also closely related to the velocity of the Bragg waves. Thus the Doppler spectrum, measured by a fixed radar, is dominated by peaks at the frequencies corresponding to the Bragg waves phase speed (Crombie 1955; Barrick 1972). The Doppler spectrum measured by the (moving) SAR is more complicated due to the non-linear mapping of the ocean wave spectrum to the SAR spectrum (K. Hasselmann and S. Hasselmann 1991).

Objectives of this thesis

The overall main goal of the work in this thesis is to demonstrate the capability of spaceborne Along-Track Interferometric SAR (ATI-SAR) in measuring sea surface currents through a number of study cases in the Baltic Sea region. This includes the investigation of the different challenges, limitations and possible errors that might hinder the quality of the measurements. The (few) previous studies using spaceborne ATI-SAR data were based on a strong known currents. The Baltic Sea region is characterised by a slow circulation, except at a few narrow straits, with no permanent strong currents. Such conditions are challenging for satellite measurements of sea surface currents.

In order to achieve the objectives, the work involves several tasks. First, it involves the

implementation of a complete interferometric processing chain, implementation of a wind model and retrieval algorithm and the implementation of a Doppler model. Second, it involves performing the comparison of the ATI-SAR currents with regional ocean circulation models such as HIROMB (SMHI) and HBM (DMI). Finally, it also includes a study of the effects impacting the current retrieval such as phase calibration, wind speed, direction, waves, etc. The assessment of the wind-wave contribution to the total radial velocity was one of the main concerns in this work. In addition, the impact of the phase processing, the Doppler model inaccuracy and the wind errors on the ATI-SAR currents is discussed in the papers. The objective is also to quantify the accuracy and the precision of the currents retrieved from ATI-SAR data, particularly critical in regions with very weak circulation. The appended papers discuss in detail each of these issues.

Interferometric Synthetic Aperture Radar (InSAR)

2

SAR principle

The geometry illustrated in figure 2.1 is called side-looking stripmap SAR and is the most used operating mode. For simplicity, only this mode is considered in this chapter.

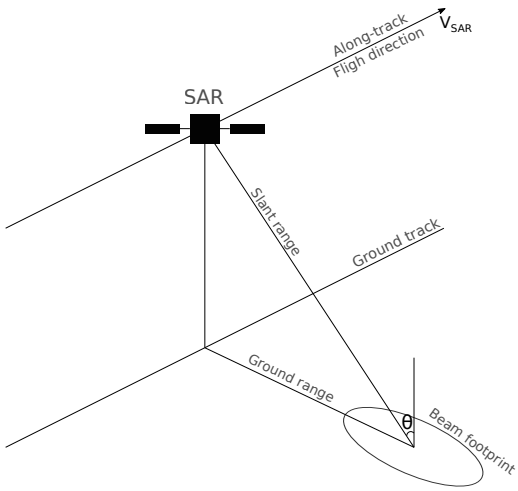

Figure 2.1. *Stripmap side-looking SAR*

There is an abundant literature about SAR, its applications and processing algorithms, see for example (Cumming and Wong 2005; Richards 2005; Ulaby and Long 2014). The main difference between SAR and RAR is the spatial resolution in the along-track direction, hence only this aspect is discussed here. Azimuth direction and along-track direction are used interchangeably in this text. In short, SAR is a technique (system+processing) to overcome the diffraction-limited resolution in the along-track direction. The angular diffraction-limited resolution $\theta_a = \lambda/D$ is determined by the wavelength λ and the antenna length in the along-track direction D. From this point of view, SAR is very similar in concept to aperture synthesis using an array of antennas.

According to the diffraction limit, the resolution can only be increased by increasing the frequency or the antenna size. SAR works around this, by transmitting and recording the scattered signal (amplitude and phase) from the targets illuminated by the antenna beam at each position on its track separated by a distance V_{SAR}/PRF, where V_{SAR} is the velocity of the platform and PRF is the pulse repetition frequency. The recorded signals are coherently integrated after compensation of the phase due to the varying distance to the target which is due to the motion of

platform (assuming static ground). This is equivalent to a long linear antenna array of (synthetic aperture) length D_{SAR}, with the main beam of the array pointing in the broadside direction toward the target location. For more details about the SAR processing, see (Cumming and Wong 2005). In terms of system design, SAR has some constraints. The PRF needs to be high enough, usually much higher than for the RAR, to avoid the azimuth ambiguities. On the other hand, this constraint limits the ground coverage in the range direction.

The achieved spatial resolution in the along-track direction is given by (Richards 2005)

$$\delta_{SAR} = \frac{R\,\lambda}{2\,D_{SAR}}\ ;\ \delta_{RAR} = \frac{R\,\lambda}{D_{RAR}}$$

Note finally, that the resolution of SAR relative to a real antenna array of the same size is improved by a factor 2. This is due to the fact that the SAR pulse is received at only one position rather than by all antenna elements.

SAR Doppler centroid

SAR processing consists mainly of two important steps; the range compression and azimuth compression. The latter is a key point in SAR performance, is more complicated and affects directly and seriously the Doppler analysis for geophysical measurements. Thus only the azimuth compression and the parameters involved are considered here.

For a SAR moving in a linear track at constant altitude, the Doppler frequency of a given static target varies approximately linearly in azimuth along the illumination time (called slow time). The Doppler frequency is the apparent shift, due to the SAR motion, in the frequency of the signal received from a given target along the slow time. The Doppler frequency at the centre of the antenna beam is called the Doppler Centroid (DC). We call this, the geometrical DC since it is only due to the geometry of the acquisition and independent of the scatterer motion. This DC is an important parameter in the SAR azimuth compression because it is used in the design of the matched filter (Cumming and Wong 2005). Inaccurate estimation of geometric DC induces a degradation in the SAR image quality. For a side looking SAR, the DC is (ideally) zero because the antenna look direction is perpendicular to the flight direction, but a non-zero DC might occur due to a beam rotation.

For spaceborne SAR as a general case, the antenna look direction needs to be perpendicular to the relative velocity of the SAR and Earth in order to obtain a zero DC. Since the DC is latitude dependent in this case, it is difficult to maintain zero DC along the satellite orbit. Many SAR platforms employ yaw steering technique (Raney 1986; Fiedler et al. 2005) in order to minimize and maintain the Doppler centroid within the unambiguous Doppler bandwidth $\pm$ PRF/2. If the SAR is looking at a moving surface, there is an additional Doppler shift, which is proportional to the velocity of the surface, that adds to the DC. The geometric DC can be estimated using the platform orbit and attitude data or from the signal (Madsen 1989; Wong and Cumming 1996). Even with the use of yaw-steering, the accuracy of the satellite position, velocity and attitude, is usually not good enough to predict accurately the geometric DC. Moreover, the Doppler centroid varies also with range and this variation needs to be modelled.

SAR interferometry principle

Interferometry is a technique used to increase the angular measurement accuracy in a given direction. This requires (at least) an additional antenna separated by a fixed (known) distance in space. To summarise, RAR locates the origin of the signal (target) in an iso-range-sphere using the time delay, SAR adds a second dimension by locating the target in the azimuth direction exploiting the Doppler shift. The intersection of the iso-range sphere and the Doppler cone is a circle. Thus a single SAR antenna is not able to locate the target in that iso-range-Doppler circle, i.e. the angle in the plane perpendicular to the flight direction is undefined. Interferometric SAR (InSAR) adds a third dimension by locating the target in elevation and measures this angle. Note that in order to distinguish two targets in the iso-range-Doppler circle more than two antennas are needed.

In SAR, the phase of the signal is directly measurable from the complex image. The phase of a single SAR measurement is related to the path length (Hanssen 2001) R as $\phi = -2kR + \phi_0$, where ϕ_0 is the scattering phase. The main assumption in InSAR is that the scatterers distribution within the pixel does not change, i.e. ϕ_0 is constant between acquisitions. Actually, InSAR still work if ϕ_0 changes slightly, the degree of change of ϕ_0 is measured by the *coherence*.

The interferometric SAR system consists of two SAR sensors looking into a common observed target area. The two antennas can be mounted on the same platform or on separate platforms. The views can differ in elevation angle (across-track interferometry) or in time (along-track interferometry). The separation between the antennas is called baseline, the choice of the baseline is application dependent. When the two platforms are close enough, bistatic imaging can be used, i.e. one transmitter and two receivers. Otherwise, monostatic imaging is used, i.e. each platform has its own transmitter and receiver.

InSAR can also be classified, depending on time separation between acquisitions, into single-pass interferometry and repeat-pass interferometry. An overview of SAR interferometry can be found in (Bamler and Hartl 1998; Rosen et al. 2000; Hanssen 2001).

Across-track interferometry

The objective of across-track interferometry is the estimation of surface elevation to construct a Digital Elevation Model (DEM). To achieve this objective two platforms must be separated in the plane perpendicular to the flight direction as illustrated in figure 2.2. In this case both single-pass and repeat-pass configurations are possible. The interferogram I is formed by co-registration of the two SAR images S_1 and S_2 and multiplying one by the complex conjugate of the other ($I = S_1 S_2^*$). The phase of the interferogram at each pixel is related to the difference in range which can be converted into height (Bamler and Hartl 1998; Rosen et al. 2000)

$$\phi_{int} = \frac{2\,\pi\,n}{\lambda}\,\Delta R \tag{2.1}$$

where $n = 1$ for bistatic and $n = 2$ for monostatic. Given that the positions of the platforms are known and the range to the target is measured from each platform, the target height can be estimated from the measured phase. Then solving for the height z becomes a geometric problem exploiting the relations (Rosen et al. 2000)

$$\Delta R = B\,sin(\theta - \alpha)$$

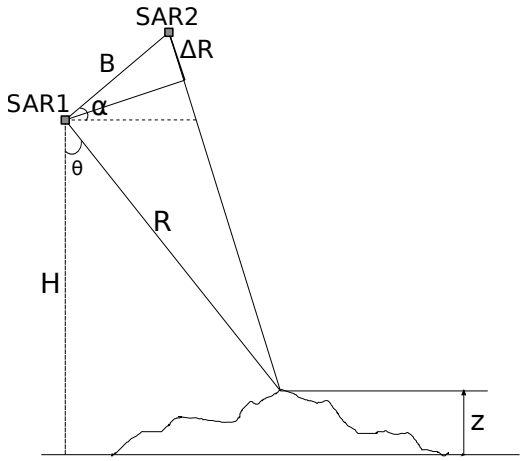

Figure 2.2. *The geometry of single pass across-track interferometry. The flight direction is perpendicular, into, the page. The antenna beam is looking to the right of the flight direction.*

$$z = H - R\,cos\theta$$

Finally, ΔR is determined from the phase using equation 2.1 and given B, calculated from the position of the platforms, θ and hence z can be determined. Note that the sensitivity of ΔR, hence the phase, to height is determined by the baseline B. Thus a larger baseline provides a better sensitivity to elevation. A larger baseline, however, reduces coherence which becomes zero at the critical baseline (Hanssen 2001).

Along-track interferometry

The objective of Along-Track Interferometry (ATI) is to measure the surface motion. The concept consists of acquiring two images of the same patch of ground at two different times as illustrated in figure 2.3. The time delay between the two acquisitions depends on the velocity of the target we want to measure and the correlation time of the imaged surface. Recall that InSAR is based on the assumption of constant scattering phase, this assumption is challenged when imaging non-rigid surfaces such forest, sea, etc. In oceanographic applications, the decorrelation time of the ocean is very short, thus the interferometric time delay should be of the order of 10 milliseconds for microwaves depending on the sea state (Tucker 1985). The ATI phase is directly related to the radial velocity of the ocean patch v_r (Ulaby and Long 2014)

$$\phi_{int} = \frac{2\,\pi\,n}{\lambda}\,\frac{B_{ATI}}{V_{SAR}}v_r \tag{2.2}$$

where B_{ATI} and V_{SAR} are the ATI baseline and the SAR velocity, respectively. Similarly to the across-track InSAR, the sensitivity of the phase to velocity depends on the baseline. Thus, longer baselines provide higher sensitivity to motion. On the other hand, a too long baseline increases the time delay and consequently decreases the *coherence*. Therefore, a compromise between

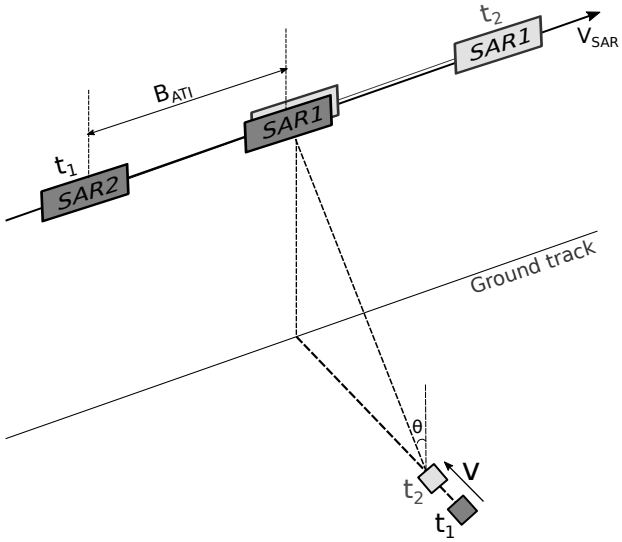

Figure 2.3. *The geometry of single pass along-track interferometry.*

coherence and sensitivity must be found. Note finally, that the ATI allows the measurement of the target velocity only in the Line-Of-Sight (LOS) or radial direction. LOS velocity and radial velocity are used interchangeably in this text. The ground range velocity is related to the radial velocity by the incidence angle θ ($v_r = v \sin\theta$).

TerraSAR-X / TanDEM-X concept

TerraSAR-X/TanDEM-X is a high-resolution interferometric SAR mission of the German Aerospace Center (DLR) (Krieger et al. 2007). The mission concept is based on an extension of the existing TerraSAR-X mission by a second satellite. Both instruments are almost identical in design and operate at X-band ($\sim 10\ GHz$) in different acquisition modes. TerraSAR-X was launched on 15 June 2007 and TanDEM-X was launched, as an add-on to TerraSAR-X, on 21 June 2010. The main application of the TanDEM-X mission is global Digital Elevation Measurement. The main orbital and system parameters are given in table 2.1.

Flying these two satellites in a close formation provides a flexible single-pass SAR interferometer configuration with configurable baseline according to the specific needs of the application. The two satellites orbit in a helix formation, which enables a safe operation of close formation with minimum collision risk (Krieger et al. 2007). The TerraSAR-X/Tandem-X interferometer is, by construction, a hybrid system, i.e. a system that combines across-track and along-track InSAR as illustrated in figure 2.4. They can operate in three different modes: Bistatic mode, Pursuit monostatic mode and Alternating bistatic mode. The data used in this thesis is from the bistatic mode. The Bistatic mode is when one satellite serves as a transmitter and both satellites, serving as receivers, record the scattered signal simultaneously.

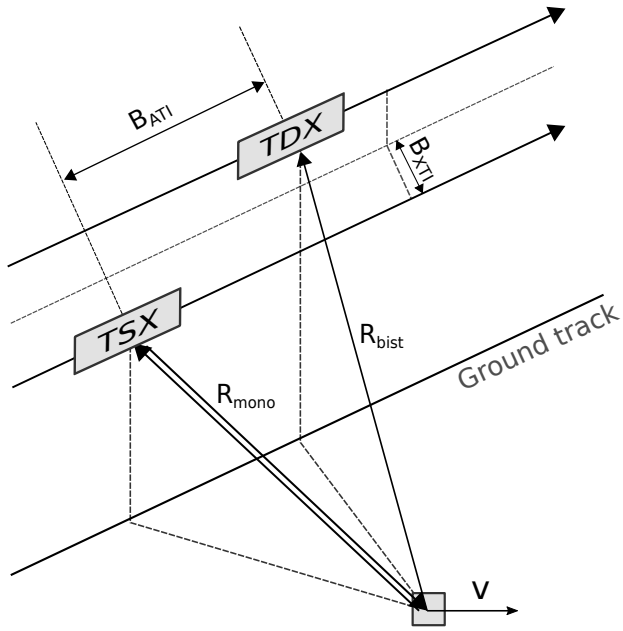

Figure 2.4. *TanDEM-X: a hybrid, single-pass and bistatic interferometric SAR.*

Orbital parameters	
Orbit Height	514 km at equator
Orbit per day	15.2/11
Orbit Repeat Cycle	11 days
Inclination	97.44 degree
Asc. node / equ. crossing time	18:00±0.25h (local time)
System parameters	
Frequency	9.65 GHz ($\lambda = 0.031\ m$)
Range bandwidth	150 MHz
Azimuth bandwidth	2.765 KHz
Range resolution	1.17 m (slant) / 2.14 m (ground)
Azimuth resolution	3.29 m

Table 2.1. *TanDEM-X orbital and system parameters*

3 Upper ocean dynamics - brief description

In this chapter a basic review of the dynamics of the upper ocean is given. For a detailed and exhaustive overview of this topic, the reader may refer to the following references (Philips 1977; Apel 1987; Kundu and Cohen 2016).

The complexity of the ocean dynamics resides in the large range of spatial and temporal scales which can differ by orders of magnitude. The ocean dynamics is driven by processes with temporal scales ranging from a fraction of a second (e.g. ripples) to hundreds of years (e.g. Global Conveyor Belt) and with spatial scales ranging from centimetres (e.g. turbulent eddies) to hundreds of kilometres (e.g. tides). Moreover, all these processes are permanently interacting with each other. The spatial and the temporal scales are generally correlated. These oceanic processes are driven by different forces but the main source of energy for the surface processes is the wind stress.

Generally speaking, SAR measures the total sea surface velocity, i.e. water parcel motion which includes many components. Recall that the objective of this work is to retrieve the sea surface current, i.e. the mean water mass transport. Thus, the other contributions (waves motion) must be well understood, estimated and removed. This task is one the main challenging problems in ocean current retrieval from SAR. The main contributions to the sea surface motion and consequently to the Doppler frequency shift observed by SAR are the surface waves and currents. In the following sections, the different contributions to the total velocity are briefly described.

Obviously, the more sources of motion we take into account, the more complicated becomes the problem. Furthermore, the degree of contribution of these different sources is not yet well understood. However, in our area of interest (Baltic Sea), the major contributions to the SAR measurements are probably the wind-driven currents, capillary wave phase speed, gravity waves orbital velocities and the Stokes drift. These sources are discussed respectively in more details in the following sections. The numerical examples given in the following sections, are very rough estimates, attempting to give an order of magnitude.

Currents

The velocity of sea surface currents is a combination of several components. These components can be classified by the causing force namely, buoyancy (thermohaline), Moon-Sun gravity (tides), pressure-gradient, wind-stress (wind drift) and wave-induced (Stokes drift). Note that the pressure gradient can also be a result of wind blowing in the same direction during a long enough time and piling up water mass. Similarly, the wave-induced is, in origin, generated by wind.

Thermohaline and wind-driven Currents

Thermohaline circulation is formed by currents driven by differences in temperature and salinity. An example of this type of circulation is the the *Global Conveyor Belt*. In simple words, thermohaline circulation is generated by the sinking of cold, salty and dense water toward the ocean bottom which gets replaced by the surface fresh and lighter water. This circulation is much slower compared to wind-driven currents, but might affect the SAR measurements.

The wind-driven currents can be classified into Ekman current (Ekman 1905), also called wind drift, and geostrophic current. The Ekman current is the direct response of the upper water layer to the local wind stress, it is a short term phenomena (few hours to few days). The geostrophic current is a relatively long-term phenomena characterised by a slow response to wind variation. In this case the motion is governed by a balance between the pressure gradient force and the Coriolis force. An Ekman current can develop into, if conditions in terms of basin size and wind duration are met, a geostrophic current.

In linear wave theory, by definition, waves transport energy but not water mass. By this definition, the average, over the wave period, of the velocity of a water particle riding the free surface of the wave is zero. This is however not true in finite amplitude wave theory or Stokes' theory. Stokes drift (Stokes 1847) is defined as the net velocity experienced by a water particle at the surface of a wave in the direction of wave propagation. The more formal definition is, the Stokes drift velocity is the difference between the average Lagrangian flow velocity of a fluid particle and the average Eulerian flow velocity of the fluid.

Sometimes in literature, the sum of wind- and wave-induced components is referred to as the total surface drift current. Estimation of the surface drift current, its relation to the wind and the contribution ratio of waves has been, and still, a topic of research. Thus many authors (J. Wu 1983; Jenkins 1987; Rascle et al. 2008; Ardhuin et al. 2009) have investigated this topic theoretically and experimentally, different results have been reported with a clear regional dependencies. However, a rule of thumb often used in literature is that the surface drift is $\approx 2-3\%$ of the wind speed and the direction is $10-45^{o}$ to the right of the wind in the Northern hemisphere (J. Wu 1983; Jenkins 1987; Ardhuin et al. 2009). Finally, there is a debate on whether radar measures Stokes drift or not and if it does how much it contributes to the total current, see e.g. (Röhrs et al. 2015).

Tides

Tides are global scale oceanic phenomena generated by the gravity of the moon and the sun, combined with a rotating Earth. They can be classified as global scale waves, but on the local scale, tides are seen as vertical motion of the sea level (tide range) and horizontal motion of water. Tidal currents, also called tidal flow or stream, refer to the periodic horizontal movement of water driven by the sea level rise induced by the tides. Thus, the velocity of the tidal current is directly related to the tide range. These currents are affected by the topography and the size of the water body. That is they are stronger in some geographic areas than others. For instance, tidal flows are stronger at estuaries/bays inlet/outlet. In open ocean, such as Atlantic and Pacific the tides are much stronger than in smaller basins such as the Mediterranean and Baltic sea. These small basins do, generally, not generate their own tides, but the Atlantic ocean tide can penetrate into them through straits.

Waves

There are several types of waves, but only the ones that are relevant to radar remote sensing are discussed here, namely gravity-capillary waves, gravity waves and internal waves. The ocean is dispersive, that is waves with different wavelengths propagate with different phase speeds. Ocean waves are characterised by their frequency w and wavelength λ. These two quantities are related by the dispersion relation (Kundu and Cohen 2016), for gravity-capillary waves

$$w^2 = \Big(g\,k + \frac{\sigma\,k^3}{\rho_w}\Big)\,tanh(kH), \tag{3.1}$$

where $\sigma,\ k$, g, ρ_w and H are, respectively, the water surface tension, the wave-number $k = 2\pi/\lambda$, the acceleration due to gravity, the water density and the water depth.

Gravity-capillary

Recall from chapter 1 that SAR signal interacts mainly with the Bragg waves. The Bragg waves for X-band radars have wavelength $\lambda_{Bragg} \approx 3\ cm$. These waves fall in the category called gravity-capillary waves or ripples which are affected by both surface tension and gravity with wavelength $\lambda \leq 7\ cm$. The phase speed c_p, of interest to SAR Doppler signal, of the capillary-gravity waves is given by $c = w/k$, using equation 3.1

$$c_p = \sqrt{\Big(\frac{\sigma k}{\rho_w} + \frac{g}{k}\Big)\,tanh(kH)}.$$

Using deep water approximation $\big(tanh(kH) \approx 1\big)$ this simplifies to

$$c_p = \sqrt{(\frac{\sigma k}{\rho_w} + \frac{g}{k})}.$$

Thus, for an X-band radar with $\lambda_r = 0.031\ m,\ \theta = 35^o,\ \lambda_{Bragg} = 0.027\ m$, and given the the following parameters $\sigma = 0.073\ Nm^{-1},\ g = 9.81\ ms^{-2},\ \rho_w = 1000$, the phase speed is $c_p = 0.24\ m/s$.

Gravity waves - Orbital velocities

Gravity waves are not affected by surface tension but only by gravity as their name refer to. These are waves with wavelength between $\approx 7\ cm$ and several hundred meters. In addition to their phase speed, waves induce orbital motion of the water particles. This orbital motion acts as a local current which advects the gravity-capillary waves, hence modulating their apparent frequency. The orbital velocity depends on the wave frequency and amplitude (Kundu and Cohen 2016). For instance, a wave with an amplitude $a = 1\ m$, period $T = 8\ s,\ (\omega = 0.78)$, the maximum orbital velocity is $u_{max} = a\omega = 0.78\ m/s$.

Internal waves

Internal waves are generated in a stratified water layers. The force generating these waves can be of multiple origins, but one important generation mechanism is a tidal flow over a rough topography. Internal waves are characterised by large periods $\geq 10\ min$, long wavelength (several hundred meters) and higher amplitudes than surface gravity waves. The phase speed is also much smaller than surface waves (≈ 30 times smaller) (Leppäranta and Myrberg 2009). Internal waves affect the SAR intensity signal, indirectly, by generating horizontal surface currents which modulate the surface Bragg waves (Alpers 1985). Internal waves-generated surface currents affect also the phase signal. They generate convergence and divergence zones on the surface due to the movement of water particles. It has been shown that non negligible surface velocities can be induced and detected by ATI-SAR (D. R. Thompson and Jensen 1993).

Baltic sea circulation

Since all the study cases investigated in this work are based on satellite images acquired over the Baltic Sea, a brief description of its circulation is given in this section. Here, the Baltic Sea includes also the Kattegat sea.

The Baltic Sea is an intra-continental, brackish water, sea with very slow water renewal with an average residence time $\approx$ 30 years (BACCII 2015). It is a relatively shallow sea with an average depth of $\approx 50\ m$. The only exchange with the North sea, through Kattegat and Skagerrak, is via the Danish straits. The fresh water supply outflows as a thin layer above the dense salty water through the Danish straits and belts. Salty water inflows from the Atlantic ocean into the Baltic sea where the fresh water mixes with the sea water. This forms the so called *Baltic haline conveyor belt* (Döös, Meier, and Döscher 2004).

The Baltic Sea does not generate its own tide due the its limited size. Moreover, the Kattegat and Danish straits are relatively narrow and shallow which limits the penetration of the oceanic tides. Since the tide velocity is related to water level changes, with amplitudes around $10\ cm$, very weak tidal currents are observed in the Baltic Sea (Leppäranta and Myrberg 2009).

The size of the Baltic Sea basins are relatively small and strong wind durations are short, hence the growth of waves is limited. Wave statistics show that the significant wave height is less than $2\ m$ and with periods less than $7\ s$ in 90% of the cases (Leppäranta and Myrberg 2009). The significant wave height is defined as four times the standard deviation of the wave height. Thus, long-period swell is rare in the Baltic Sea. Internal waves depend on the density stratification. The Baltic Sea with a stable stratification, provides a background for internal waves development. Thus, these are commonly observed. These internal waves are not driven by tides.

Finally, The Baltic Sea has no noticeable permanent and stable current structures such as the Gulf stream in the Atlantic ocean. There is, however, a net (long term mean) flow to the south on the west side of the Baltic sea, generating a large, slow, southerly coastal current along Sweden's coast (Leppäranta and Myrberg 2009). These currents are very weak with a mean average speeds of $\approx\ 5\ cm\ s^{-1}$, whereas wind drift currents, during storms, can reach $50\ cm\ s^{-1}$ (Leppäranta and Myrberg 2009).

How SAR "sees" waves and currents

Backscatter modulation

As mentioned in previous sections, SAR measures mainly the backscattered power from the Bragg waves. In principle, it does not directly "see" the long ($\lambda_w \geq n\ \lambda_{Bragg}$) waves. There is a debate about the definition of long waves in SAR ocean remote sensing literature, but generally n is between 3 and 10. Long waves are detected, indirectly, by SAR (Alpers, Ross, and Rufenach 1981), based on three mechanisms, namely tilt modulation, hydrodynamic modulation and velocity bunching (Elachi and Brown 1977; K. Hasselmann, Raney, et al. 1985).

A complete description of these mechanisms is beyond the scope of this thesis (For a more details see for example (Robinson 2004)), but here follows a brief description. Tilt modulation is the modification of the local incidence angle by the slopes of the long waves. A backscatter model which takes into account the Bragg scattering and the tilt modulation is called the two-scale model (Valenzuela 1968). The two scale refers to approximating the sea surface as Bragg patches (also called roughness facets, small scale) tilted and modulated by the slopes and velocities of the long waves (large scale). Hydrodynamic modulation is due to the straining and stretching of the Bragg waves by the long waves orbital velocities. This leads to an enhanced backscatter at the leading front of the waves and weaker backscatter at the trailing front. Moreover, the hydrodynamic modulation yields a different modulation depending on the wave propagation direction. This is actually the only mechanism allowing the radar to distinguish between the upwind and downwind direction. Velocity bunching is due to the fact that SAR imaging/processing is based on static targets. Thus, waves in motion will be non-uniformly displaced in azimuth direction, i.e. different roughness patches along the wave have different velocities (positive and negative).

The surface currents are also imaged by SAR based on the hydrodynamic modulation mechanism. In fact, SAR images the current gradient, i.e. a constant current will not change the backscatter. Similar to the long waves, current spatial variation generates convergence and divergence zones of the surface roughness hence the modulation of the backscatter. The amplitude of this modulation depends on the relative direction between the wave propagation direction and the current. Finally, internal waves (Alpers 1985) and sea floor topography (Alpers and Hennings 1984) are also imaged by the similar mechanism (hydrodynamic modulation).

Doppler modulation

A patch of roughness (also called facet) is advected by the long waves orbital velocities and currents. This will affect the Doppler frequency shift measured by the SAR. The mean Doppler frequency shift f_D of a given surface area is the spatial average of the radial velocity of the scatterers, weighted by the local σ^0 (Chapron, Collard, and Ardhuin 2005; Johannessen, Chapron, et al. 2008)

$$f_D = -\frac{k_e}{\pi}\, U_D = -\frac{k_e}{\pi}\, \frac{\overline{v_r\ \sigma^0(\theta + \Delta\theta_I)}}{\overline{\sigma^0(\theta_I + \Delta\theta)}} \tag{3.2}$$

where $v_r = u\ sin\theta - w\ cos\theta$, u and w are the horizontal and vertical components of the scatterer (facet) velocity and θ_I is the local incidence angle. Note that u and w include the phase speed of the Bragg waves, and the advection by the long waves orbital velocity and any possible current.

The correlation between the modulation of the NRCS and the modulation of the facet velocity yields a net velocity, also called velocity bias, in the direction of the propagation of the wave (Chapron, Collard, and Ardhuin 2005; Romeiser and D. R. Thompson 2000). In other words, for instance along a wave propagating away from the satellite, a facet tilted toward the satellite will have a higher backscatter and negative velocity while a facet tilted away will have smaller backscatter. This yields a shift of the Doppler spectrum toward negative frequencies.

Finally in addition to shifting the Doppler spectrum the orbital motion of the long waves will broaden the spectral lines at the Bragg frequencies (Plant and Keller 1990; Romeiser and D. R. Thompson 2000). This broadening is more important at high frequencies, e.g. X-band because the number of the long modulating waves is larger.

4

State of the Art

Observing sea surface currents

There are several radar based techniques for measuring ocean currents. One of the most established techniques is using coastal High Frequency (HF) radars (Barrick 1972). The advantage of HF radar is its simplicity, but the drawback is their sparsity. Moreover, the coverage is limited to some $100\ km$ from the coastline and the spatial resolution is coarse $\sim 2-5\ km$. Another well established technique is using satellite altimeters. This has also a coarse spatial resolution ($\sim 10\ km$) and they measure only the geostrophic component of the ocean current. SAR complements these measuring techniques by offering very high resolution observations ($\leq\ 100\ m$) , particularly important in coastal regions characterised by small scale processes.

Remote sensing techniques of surface currents from spaceborne SAR can be classified in two categories, namely feature-tracking-based or Doppler-based techniques. An ocean feature here refers to anthropogenic, e.g. oil or biological, e.g. algae surfactant. The feature tracking technique is based on using sequential SAR images (Lyzenga and Marmorino 1998) and measuring the correlation between the two images. This measure of correlation can be related, given the time between the two acquisition is known, to the surface motion.

The Doppler-based technique can be split in two different techniques which are quite similar in principle, but differ in design, implementation and performance. A good review for sea surface currents imaging by spaceborne SAR using both techniques can be found in (Romeiser, Johannessen, et al. 2010). The first technique is called the Doppler Centroid Anomaly (DCA) and is based on the difference between the measured and the geometric Doppler centroid (see section 2.2). The DCA was first introduced and demonstrated by (Chapron, Collard, and Ardhuin 2005) and then by (Hansen et al. 2011) for example. The advantage of the DCA is that it requires one SAR image only. The drawback is its relatively coarse resolution ($\approx 1-2\ km$), which is still much better than the altimeter resolution though.

The second technique is based on SAR along-track interferometry (see section 2.5) which requires two SAR acquisitions. This technique was first introduced and demonstrated by (Goldstein and Zebker 1987; Goldstein, Zebker, and Barnett 1989). The advantage of using ATI-SAR for sea surface current mapping is its high spatial resolution ($\approx 100\ m$). Such high resolution current maps would be particularly important in coastal areas, rivers, straits, etc. This technique is the main topic of this thesis, thus it is discussed in full details through the appended papers.

Analysis Methods

Interferogram processing

Interferogram processing consists of the following steps. First, the two complex images are co-registred in space. Second, the interferogram is calculated from the complex correlation of the two images as

$$\gamma = \frac{E\{s_1 s_2 *\}}{\sqrt{E\{|s_1|^2\}E\{|s_2|^2\}}} \tag{4.1}$$

The coherence is defined as the magnitude of γ and the phase is the argument of γ. In order to reduce the random phase noise, spatial averaging is usually performed. Third, the removal of the flat Earth phase (interferogram flattening) is carried out. A spatial filtering (median filter) might be needed to filter out targets such as ships and wind turbines in the sea. If phase wrapping occurs then phase unwrapping is performed. Fourth, the phase is calibrated if land is present in the image. This step is discussed in full details in the papers 2 and 4. Fifth, the image is mapped from SAR coordinates to Earth geographic coordinates (geocoding). Finally, the phase is converted to radial velocity provided the along-track-baseline and the velocity of the satellite are known. The main outputs of the ATI processing chain are the NRCS, the coherence and the interferometric phase.

Wind retrieval

It can be noticed by reading this thesis and the appended papers that ocean currents retrieval is highly dependent on wind speed and direction. Therefore, wind retrieval is a determinant component in ocean currents retrieval.

Wind speed

Wind speed retrieval is an inversion problem. Like any inversion problem, a forward model is needed. The forward models used in wind retrieval are generally empirical and following the scatterometry terminology, they are called Geophysical Model Functions (GMF). They relate the wind speed and direction to σ^0 as

$$\sigma^0 = GMF(\theta, V, \phi, f, pol) \tag{4.2}$$

where V is the wind speed, ϕ is the angle between the wind direction and the antenna beam, θ is the incidence angle, f is the frequency and pol is the polarisation.

The XMOD2 GMF (Li and Lehner 2014), data is used in this study and is depicted in figure 4.1. It has a similar mathematical formulation as the CMOD GMF series

$$\sigma^0 = B_0(1 + B_1 cos(\phi) + B_2 cos(\phi))^{1.6} \tag{4.3}$$

Before wind retrieval the backscatter needs to be calibrated as follows

$$\sigma^0 = K|DN|^2 sin(\theta) - NESZ \tag{4.4}$$

Where K, DN, θ and $NESZ$ are calibration factor, digital number, incidence angle and Noise Equivalent Sigma Zero respectively. The wind direction is obtained from another source, e.g. numerical weather prediction model.

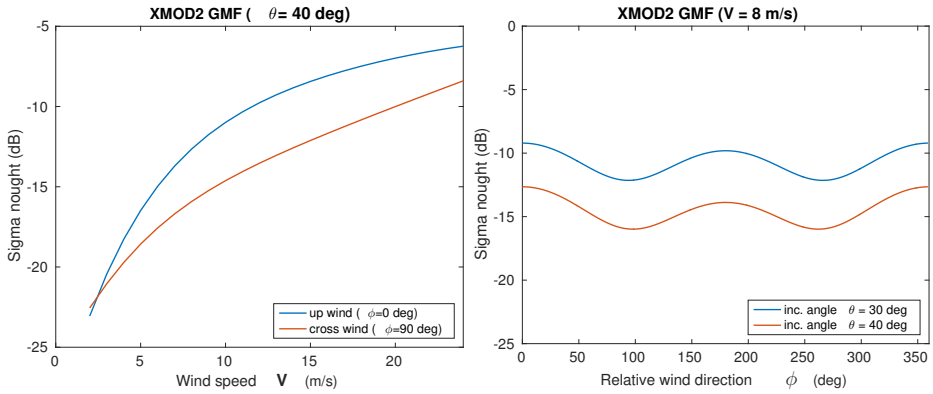

Figure 4.1. *Wind model - XMOD2 GMF*

The solution to the inversion problem is finding the wind speed that minimises the cost function

$$J(V) = \sum_i (\sigma^0_{meas_i} - GMF(V, \phi, \theta))^2 \tag{4.5}$$

Where V, ϕ, θ and σ^0_{meas} are the wind speed, wind direction, incidence angle and the measured backscatter. The sum is ideally an ensemble average if different measurements are available or a spatial average.

Wind direction

In the previous section, it is assumed that the wind direction is provided by an external source such an atmospheric model. It is also possible to extract the wind direction directly from the SAR image (Wackerman et al. 1996; Koch 2004). The underlying assumption is that Languimir circulation cells in the surface layer and atmospheric roll vortices induce convergence/divergence bands parallel to the wind direction (Gerling 1986; Alpers and Brummer 1994). This wind direction extraction is based on the detection of these features (convergence/divergence bands) and their alignment. This is achieved by edge detection techniques in the spatial domain such as Local Gradient (LG) technique (Wackerman et al. 1996; Koch 2004) or in the spectral domain using Fourier transform (Wackerman et al. 1996). The LG technique is used in this work.

Wind-wave removal

As discussed in section 3.4, even in the absence of ocean currents, the ATI Doppler velocity will contain a contribution from waves motion. Moreover, this contribution is often larger than the proper current (water mass transport) contribution (see papers 1 and 4 for more details). Thus, in order to retrieve the ocean currents from ATI-SAR, this wave contribution need to be estimated and removed. This can be achieved by using a Doppler model. This model simulates what the Doppler shift SAR would measure from wave motion for a given a wind speed and direction. This

Doppler GMF has the form

$$f_{DOP} = GMF(\theta, V_W, \phi_W, f, pol) \tag{4.6}$$

where the arguments of the Doppler GMF have the same definition as the arguments of the wind GMF in equation 4.2.

A theoretical model, called M4S, was developed by (Romeiser and D. R. Thompson 2000)) and an empirical model, called CDOP, was developed by (Mouche et al. 2012) for C-band. For instance, the variation of CDOP with wind speed and direction is illustrated in figure 4.2.

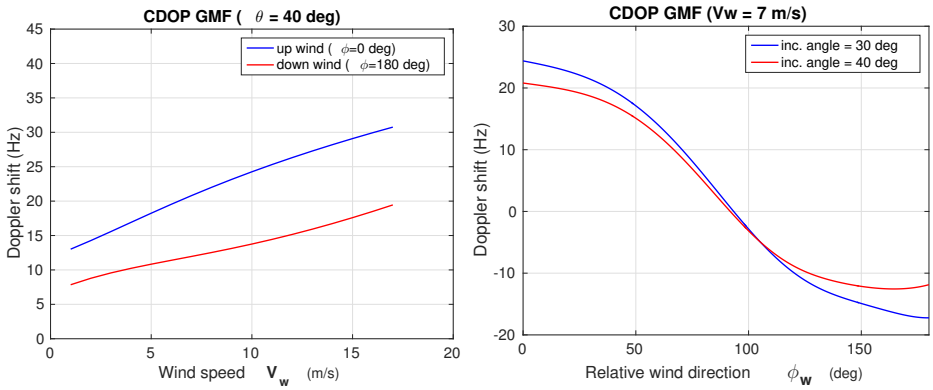

Figure 4.2. *Doppler model - CDOP GMF*

Finally, the simulated Doppler shift is subtracted from the measured Doppler shift as

$$f_{D_{current}} = f_{D_{meas}} - GMF(\theta, V_W, \phi_W, f, pol)$$

Note that this assumes the advection effect and does not take into account the wave-current interaction which consists of the modulation of the wave spectrum by the currents gradient. Discussion of this topic is beyond the scope of this thesis, for more details see (Romeiser and D. R. Thompson 2000).

5 Summary of Appended Papers

Paper A: Wind-wave Effect on ATI-SAR measurements of ocean surface currents in the Baltic Sea

Usually the simulated SAR images were done using wind vectors provided by atmospheric models which have very coarse spatial resolution ($\sim 5 - 10\ km$). Thus, the simulated images were also very coarse and didn't reproduce the spatial variability of the measured quantity, e.g. σ^0. This paper shows that retrieving the wind speed from the SAR backscatter using an empirical model improves significantly the simulated images. This was demonstrated using the M4S SAR simulator. A comparison of the coherence and phase images simulated using SAR-winds against model winds shows small scale features not resolved by the model and the images simulated using SAR winds are much more similar to the measured SAR images.

Paper B: Phase calibration of TanDEM-X ATI-SAR data for sea surface velocity measurements

TanDEM-X formation is a hybrid system combining across- and along-track interferometry. It was found that after flat Earth phase removal the phase over static targets (e.g. land) with negligible height was not zero. This indicates that the phase is biased and needs to be calibrated. In this paper we proposed a method to calibrate the interferometric phase using land. A Digital Elevation Model (DEM) is used to remove the across-track component leaving only the along-track component. The residual phase is averaged over all land pixels (increasing the estimate precision) and the mean bias is removed from all the image. It is shown that this method provides more realistic and plausible surface velocities.

Paper C: Wind Direction Ambiguity Removal Using Along-Track INSAR: A Case Study

In contrast to scatterometers which do measurements in several directions, SAR uses a single antenna, which hinders the retrieval of the wind vectors. The main obstacle in the retrieval of wind direction from SAR data is resolving the 180 ^{o} ambiguity. Few methods have been suggested in literature for the wind direction retrieval based on feature detection in the backscatter image. Most of these methods have to rely on atmospheric models to resolve the ambiguity constraining the final spatial resolution of the wind product. In this paper, we propose a method to resolve this ambiguity without using any external source of information. We show that in case of

interferometric SAR the ambiguity can be resolved using the interferometric phase. This is based on the fact that wind-wave contribution to the phase is very often dominant.

Paper D: Measurements of Sea Surface Currents in the Baltic Sea Region using Spaceborne Along-Track InSAR

Most of the published ATI-SAR demonstrations have been carried out in areas with known and strong currents ($\geq 1\ m/s$). In this paper, we demonstrate the capability of ATI-SAR to measure ocean surface currents in conditions that are very challenging, in terms of precision and accuracy. The study area in this paper has no permanent nor strong currents and it is rather characterised by weak circulation with current speeds $\leq 0.5\ m/s$. We found that the wind-wave motion contribution is systematically dominant. We propose a simple wave contribution removal based on a Doppler model. A quantitative comparison of the retrieved currents and an ocean circulation model is performed. We have found that current retrieval is very sensitive to wind speed and direction. It was shown that by applying the appropriate processing and corrections a good agreement with the ocean model is achieved.

6 Conclusion and Future Work

Conclusion

The work in this thesis involves the implementation of a full interferometry processing chain for TanDEM-X data. This also involves the implementation of a wind model (XMOD2), wind retrieval algorithm and a Doppler model (M4S). After analysing several TanDEM-X acquisitions, it was observed that wind-waves motion is the dominant contribution to the ATI-SAR phase. Several simulations of the backscatter and the phase using the M4S model were carried out. It was found that using wind speed retrieved from SAR, rather than using atmospheric model wind data, improves significantly the simulation. Through several study cases, acquired over the Baltic Sea, we have demonstrated that a spaceborne ATI-SAR system such as TanDEM-X is capable of measuring very weak ocean currents ($\sim\ 0.3\ m\ s^{-1}$). We have shown that this requires a highly accurate phase processing. We further found that ocean currents retrieval is particularly sensitive to wind errors. Thus, by applying the appropriate corrections a good accuracy is achieved ($\sim\ 0.1\ m\ s^{-1}$). Finally, we have shown that the ATI phase can be used to remove the wind direction ambiguity extracted from SAR. This is a problematic limitation that hinders SAR wind vector retrieval.

Future

In the present work, the ATI current measurements were compared to the ocean circulation models, HIROMB and HBM. These models have a coarse resolution ($\sim\ 2\ km$). In the future, a high resolution set-up of an ocean model, based on MITgcm for the Öresund region, is ongoing in collaboration with Gothenburg University. So far, a simple wind retrieval method is adopted, but given the importance of wind information in ocean current retrieval, an improvement of the wind retrieval algorithm is planned. The improvement involves introducing a Bayesian scheme (prior information) and using the direction extraction augmented with the ATI phase for ambiguity removal. Since we found differences between Doppler models, there is a motivation to develop an empirical Doppler model from TanDEM-X data. We would also like to explore other Doppler based technique (DCA) and other satellite data, e.g. Sentinel-1, Radarsat-2, etc. Finally, comparisons with coastal HF radars and in-situ data, when temporal and spatial collocation with satellite data is available, will be performed.

References

Alpers, W. (1985). Theory of radar imaging of internal waves. *Nature Letters*, vol. 314, pp. 245–247.

Alpers, W. and Brummer, B. (1994). Atmospheric boundary layer rolls observed by the synthetic aperture radar aboard the ERS-1 satellite. *Journal of Geophysical Research*, vol. 99, no. C6, pp. 12613–12621.

Alpers, W. and Hennings, Ingo (1984). A theory of the imaging mechanism of underwater bottom topography by real and synthetic aperture radar. *Journal of Geophysical Research: Oceans*, vol. 89, no. C6, pp. 10529–10546.

Alpers, W., Ross, Duncan B., and Rufenach, Clifford L. (1981). On the detectability of ocean surface waves by real and synthetic aperture radar. *Journal of Geophysical Research: Oceans*, vol. 86, no. C7, pp. 6481–6498.

Apel, John. (1987). *Principles of ocean physics*. 1st ed. Academic Press.

Ardhuin, Fabrice et al. (2009). Observation and estimation of Lagrangian, Stokes, and Eulerian currents induced by wind and waves at the sea surface. *Journal of Physical Oceanography*, vol. 39, no. 11, pp. 2820–2838.

BACCII (2015). *Second assessment of climate change for the baltic sea basin*. Springer, Cham.

Bamler, Richard and Hartl, Philipp (1998). Synthetic aperture radar interferometry. *Inverse Problems*, vol. 14, no. 4, R1.

Barrick, D. (1972). First-order theory and analysis of mf/hf/vhf scatter from the sea. *IEEE Transactions on Antennas and Propagation*, vol. 20, no. 1, pp. 2–10.

Bentamy, Abderrahim et al. (2017). Homogenization of scatterometer wind retrievals. *International Journal of Climatology*, vol. 37, no. 2, pp. 870–889.

Chapron, B., Collard, F., and Ardhuin, Fabrice (2005). Direct measurements of ocean surface velocity from space: interpretation and validation. *Journal of Geophysical Research*, vol. 110.

Cox, Charles and Munk, Walter (1954). Measurement of the roughness of the sea surface from photographs of the sun's glitter. *Journal of the Optical Society of America*, vol. 44, no. 11, pp. 838–850.

Crombie, D. D. (1955). Doppler spectrum of sea echo at 13.56 mc./s. *Nature*, vol. 175, pp. 681–682.

Cumming, Ian G. and Wong, Frank H. (2005). *Digital processing of synthetic aperture radar data: algorithms and implementation*. Boston, London: Artech House Inc.

Dagestad, Knut-Frode et al. (2012). "Wind retrieval from synthetic aperture radar - an overview". Proceedings of SEASAR 2012.

Dawe, Jordan T. and Thompson, Lu A. (2006). Effect of ocean surface currents on wind stress, heat flux, and wind power input to the ocean. *Geophysical Research Letters*, vol. 33, no. 9.

DeVries, Tim, Holzer, Mark, and Primeau, Francois (2017). Recent increase in oceanic carbon uptake driven by weaker upper-ocean overturning. *Nature*, vol. 542, pp. 215–218.

Döös, K., Meier, H. E., and Döscher, R. (2004). The baltic haline conveyor belt or the overturning circulation and mixing in the baltic. *Ambio*, vol. 33, no. 4-5.

Ekman, Vagn Walfrid (1905). On the influence of the earth's rotation on ocean-currents. *Arkiv. Mat. Astr. Fys.*, vol. 1, pp. 1–53.

Elachi, C. (1978). Radar imaging of the ocean surface. *Boundary-Layer Meteorology*, vol. 13, no. 1, pp. 165–179.

Elachi, C. and Brown, W. (1977). Models of radar imaging of the ocean surface waves. *IEEE Journal of Oceanic Engineering*, vol. 2, no. 1, pp. 84–95.

Engen, G. et al. (1994). Directional wave spectra by inversion of ERS-1 synthetic aperture radar ocean imagery. *IEEE Transactions on Geoscience and Remote Sensing*, vol. 32, no. 2, pp. 340–352.

Fiedler, Hauke et al. (2005). Total zero doppler steering - a new method for minimizing the doppler centroid. *IEEE Geoscience and Remote Sensing Letters*, vol. 2, pp. 141–145.

Fletcher, Sara E. Mikaloff (2017). Climate science: Ocean circulation drove increase in CO2 uptake. *Nature*, vol. 542, pp. 169–170.

Gens, Rudi (2008). Oceanographic applications of sar remote sensing. *GIScience and Remote Sensing*, vol. 45, no. 3, pp. 275–305.

Gerling, T. W. (1986). Structure of the surface wind field from the seasat SAR. *Journal of Geophysical Research*, vol. 91, no. C2, pp. 2308–2320.

Goldstein, R.M. and Zebker, H.A. (1987). Interferometric radar measurement of ocean surface currents. *Nature*, vol. 328, pp. 707–709.

Goldstein, R.M., Zebker, H.A., and Barnett, T. P. (1989). Remote sensing of ocean currents. *Science*, vol. 246 (4935), pp. 1282–1285.

Hansen, M. W. et al. (2011). Retrieval of sea surface range velocities from Envisat ASAR doppler centroid measurements. *IEEE Transactions on Geoscience and Remote Sensing*, vol. 49, no. 10, pp. 3582–3592.

Hanssen, Ramon F. (2001). *Radar interferometry: data interpretation and error analysis*. 1st ed. Springer.

Hasselmann, K. and Hasselmann, S. (1991). On the nonlinear mapping of an ocean wave spectrum into a synthetic aperture radar image spectrum and its inversion. *Journal of Geophysical Research: Oceans*, vol. 96, no. C6, pp. 10713–10729.

Hasselmann, K., Raney, R. K., et al. (1985). Theory of synthetic aperture radar ocean imaging: a marsen view. *Journal of Geophysical Research: Oceans*, vol. 90, no. C3, pp. 4659–4686.

Horstmann, J. et al. (2003). Global wind speed retrieval from sar. *IEEE Transactions on Geoscience and Remote Sensing*, vol. 41, no. 10, pp. 2277–2286.

IPCC (2013). *Ipcc, 2013: climate change 2013: the physical science basis. contribution of working group i to the fifth assessment report of the intergovernmental panel on climate change*. Tech. rep. IPCC.

Jenkins, Alastair D. (1987). Wind and wave induced currents in a rotating sea with depth-varying eddy viscosity. *Journal of Physical Oceanography*, vol. 17, no. 7, pp. 938–951.

Johannessen, J. A., Chapron, B., et al. (2008). Direct ocean surface velocity measurements from space: improved quantitative interpretation of Envisat ASAR observations. *Geophysical Research Letters*, vol. 35, no. 22.

Johannessen, J. A., Kudryavtsev, V., et al. (2005). On radar imaging of current features: 2. mesoscale eddy and current front detection. *Journal of Geophysical Research: Oceans*, vol. 110, no. C7.

Kerbaol, V. and Collard, F. (2005). Sar-derived coastal and marine applications: from research to operational products. *IEEE Journal of Oceanic Engineering*, vol. 30, no. 3, pp. 472–486.

Koch, W. (2004). Directional analysis of SAR images aiming at wind direction. *IEEE Transactions on Geoscience and Remote Sensing*, vol. 42, no. 4, pp. 702–710.

Krieger, G. et al. (2007). TanDEM-X: a satellite formation for high-resolution SAR interferometry. *IEEE Transactions on Geoscience and Remote Sensing*, vol. 45, no. 11, pp. 3317–3341.

Kudryavtsev, V. et al. (2005). On radar imaging of current features: 1. model and comparison with observations. *Journal of Geophysical Research: Oceans*, vol. 110, no. C7.

Kundu, Pijush K. and Cohen, Ira M. (2016). *Fluid mechanics*. 6th ed. Elsvier.

Leppäranta, Matti and Myrberg, Kai (2009). *Physical Oceanography of the Baltic Sea*. 1st ed. Springer.

Li, X. M. and Lehner, S. (2014). Algorithm for sea surface wind retrieval from TerraSAR-X and TanDEM-X data. *IEEE Transactions on Geoscience and Remote Sensing*, vol. 52, no. 5, pp. 2928–2938.

Lyzenga, David R. and Marmorino, George O. (1998). Measurement of surface currents using sequential synthetic aperture radar images of slick patterns near the edge of the gulf stream. *Journal of Geophysical Research: Oceans*, vol. 103, no. C9, pp. 18769–18777.

Madsen, S. Nørvang (1989). Estimating the Doppler centroid of SAR data. *IEEE Transactions on Aerospace and Electronic Systems*, vol. 25(2), pp. 134–140.

Mouche, A. et al. (2012). On the use of Doppler shift for sea surface wind retrieval from SAR. *IEEE Transactions on Geoscience and Remote Sensing*, vol. 50, no. 7, pp. 2901–2909.

NOAA (2016). *Report on modeling oceanic transport of floating marine debris*. Tech. rep. NOAA.

Philips, O. M. (1977). *The dynamics of the upper ocean*. 2nd ed. Cambridge University Press.

Plant, W. J. (1990). Bragg scattering of electromagnetic waves from the air/sea interface. *Surface Waves and Fluxes: Volume II — Remote Sensing*. Ed. by G. L. Geernaert and W. L. Plant. Springer Netherlands, pp. 41–108.

Plant, W. J. and Keller, W. C. (1990). Evidence of bragg scattering in microwave doppler spectra of sea return. *Journal of Geophysical Research: Oceans*, vol. 95, no. C9, pp. 16299–16310.

Raney, R. K. (1986). Doppler properties of radars in circular orbits. *International Journal of Remote Sensing*, vol. 7, no. 9, pp. 1153–1162.

Rascle, Nicolas et al. (2008). A global wave parameter database for geophysical applications. part 1: wave-current–turbulence interaction parameters for the open ocean based on traditional parameterizations. *Ocean Modelling*, vol. 25, no. 3, pp. 154–171.

Richards, Mark A. (2005). *Fundamentals of Radar Signal Processing*. Ed. by Mark Richards. McGraw-Hill.

Richards, Mark A., Scheer, James A., and Holm, William A. (2010). *Principles of Modern Radar: Basic Principles*. SciTech Publishin.

Robinson, Ian S. (2004). *Measuring the oceans from space*. 1st ed. Springer.

Röhrs, Johannes et al. (2015). Comparison of hf radar measurements with eulerian and lagrangian surface currents. *Ocean Dynamics*, vol. 65, no. 5, pp. 679–690.

Romeiser, R., Johannessen, J. A., et al. (2010). Direct surface current field imaging from space by along-track InSAR and conventional SAR. *Oceanography from Space, Revisited*. Ed. by V. Barale, J. F. R. Grower, and L. Alberotanza. Springer. Chap. 5, pp. 73–91.

Romeiser, R. and Thompson, D. R. (2000). Numerical study on the along-track interferometric radar imaging mechanism of oceanic surface currents. *IEEE Transactions on Geoscience and Remote Sensing. Vol. 38-II, 446-458, 2000.*, vol. 38, no. 2, pp. 446–458.

Rosen, P. A. et al. (2000). Synthetic aperture radar interferometry. *Proceedings of the IEEE*, vol. 88, no. 3, pp. 333–382.

SchulzStellenfleth, J., König, T., and Lehner, S. (2007). An empirical approach for the retrieval of integral ocean wave parameters from synthetic aperture radar data. *Journal of Geophysical Research: Oceans*, vol. 112, no. C3.

Stoffelen, A. and Anderson, D.L.T. (1993). Wind retrieval and ERS-1 scatterometer radar backscatter measurements. *Advances in Space Research*, vol. 13, no. 5, pp. 53–60.

Stokes, George Gabriel (1847). On the theory of oscillatory waves. *Mathematical and physical papers*. Vol. 8. Cambridge Library Collection - Mathematics. Cambridge University Press, pp. 197–229.

Thompson, D. R. and Jensen, J. R. (1993). Synthetic aperture radar interferometry applied to ship generated internal waves in the 1989 Loch Linnhe experiment. *Journal of Geophysical Research: Oceans*, vol. 98, no. C6, pp. 10259–10269.

Tucker, M. J. (1985). The decorrelation time of microwave radar echoes from the sea surface. *International Journal of Remote Sensing*, vol. 6, no. 7, pp. 1075–1089.

Ulaby, Fawwaz T. and Long, David G. (2014). *Microwave radar and radiometric remote sensing*. 1st ed. The University of Michigan press.

Ulaby, Fawwaz T., Moore, Richard K., and Fung, Adrian K. (1986). *Microwave remote sensing: active and passive, volume ii: radar remote sensing and surface scattering and emission theory*. 1st ed. Artech House.

Valenzuela, G. R. (1968). Scattering of electromagnetic waves from a tilted slightly rough surface. *Radio Science*, vol. 3, no. 11, pp. 1057–1066.

Valenzuela, G. R. (1978). Theories for the interaction of electromagnetic and oceanic waves — a review. *Boundary-Layer Meteorology*, vol. 13, no. 1, pp. 61–85.

Wackerman, C. C. et al. (1996). Wind vector retrieval using ERS-1 synthetic aperture radar imagery. *IEEE Transactions on Geoscience and Remote Sensing*, vol. 34, no. 6, pp. 1342–1352.

Winton, Michael et al. (2013). Connecting changing ocean circulation with changing climate. *Journal of Climate*, vol. 26, no. 7, pp. 2268–2278.

Wong, Frank H. and Cumming, Ian G. (1996). A combined SAR Doppler centroid estimation scheme based upon signal phase. *IEEE Transactions on Geoscience and Remote Sensing*, vol. 34, no. 3, pp. 696–707.

Wright, J. (1966). Backscattering from capillary waves with application to sea clutter. *IEEE Transactions on Antennas and Propagation*, vol. 14, no. 6, pp. 749–754.

Wu, Jin (1983). Sea-surface drift currents induced by wind and waves. *Journal of Physical Oceanography*, vol. 13, no. 8, pp. 1441–1451.

Wu, Yang, Zhai, Xiaoming, and Wang, Zhaomin (2017). Decadal-mean impact of including ocean surface currents in bulk formulas on surface air–sea fluxes and ocean general circulation. *Journal of Climate*, vol. 30, no. 23, pp. 9511–9525.